Supporting information for:

One more attempt on ArXe

Elke Fasshauer,[*,†] Melanie Mucke,[‡,‖] Marko Förstel,[‡,⊥] ...,[¶] and Uwe

Hergenhahn[*,¶]

Centre for Theoretical and Computational Chemistry, Department of Chemistry, University
of Tromsø– The Arctic University of Norway, N-9037 Tromsø, Norway,
Max-Planck-Institute for Plasma Physics, Boltzmannstr. 2, 85748 Garching, Germany,
Max-Planck-Institute for Plasma Physics, Wendelsteinstr. 1, 14791 Greifswald, Germany,
and

E-mail: elke.fasshauer@uit.no; uwe.hergenhahn@ipp.mpg.de

---

[*]To whom correspondence should be addressed
[†]UIT
[‡]IPP
[¶]IPP HGW
[§]IOM
[‖]Now at: Department of Physics and Astronomy, Uppsala University, Box 516, 75120 Uppsala, Sweden
[⊥]Now at: University of Hawai'i at Manoa, 2545 McCarthy Mall, 96816 HI Honolulu, USA
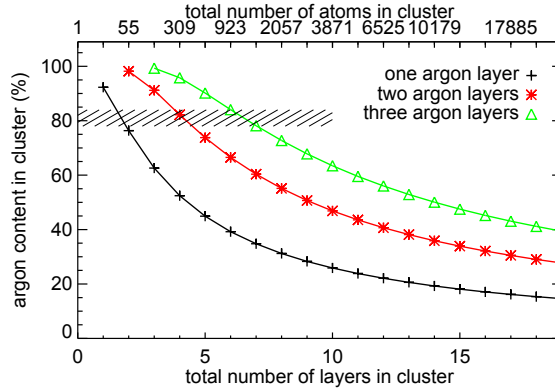
Composition of core-shell clusters

Figure S1: Argon content of ideal icosaedric Xe-core, Ar-shell systems. The relative number of surface atoms decreases with increasing cluster size. The hatched area corresponds to the Ar content of the largest clusters produced in our experiments (label 'XL').

For icosaedric clusters, the number of atoms in every shell is given.[?] For a core-shell system in this ideal geometry, the relative content of both species can therefore readily be calculated. In Figure S1 we draw the Ar content of Xe-core, Ar-shell systems with one, two and three full Ar outer layers. A comparison of these graphs with Tables 1 and 3 of the main article shows that the largest clusters produced in our experiments ('XL'), for which a core-shell structure is probable, may have between 923 and 1415 atoms in total, corresponding to three and four Xe shells around a central Xe atom, followed by three Ar outer layers. The Xe content for these systems is 0.16 and 0.22, resp.

Electron-electron coincidence spectra

In this work, we use electron-electron coincidence spectroscopy to isolate electrons from autoionization decays of Ar $3s^{-1}$ vacancies from the remainder of the electron spectrum, mostly photoelectrons from outer valence levels and secondary electrons from intracluster inelastic collisions. By recording two electrons ejected in the same process, on an event-by-event basis, we are able to identify those secondary electrons which are ejected after Ar

3s photoionization. Here, we show a more detailed representation of the electron-electron coincidence data, from which figures in the main paper showing the ICD/ETMD spectra, and the pertaining Ar 3s photoelectron spectra, were derived.

A necessary condition for the ejection of two electrons by a single photon, irrespective of the mechanism by which this is accomplished, is a sufficient photon energy. In case of a sequential process, such as photoionization followed by ICD/ETMD, moreover the ionic state which is produced in the primary step must be located above the ionization threshold for the doubly ionized systems. For Ar 3s autoionization, these conditions are discussed in detail in the main paper. For a general double ionization process, the required energy can be estimated as the sum of the single ionization energies of the final state holes (main paper, Table 3) plus the geometry-dependent Coulomb repulsion (main paper, Figure 1). Roughly, 27 eV are needed to produce an Ar $3p^{-1}$ Xe $5p_{3/2}^{-1}$ state, and about 2-4 eV less for (Xe $5p^{-1})_2$ states. For photon energies exceeding this limit, the excess energy can be distributed to any, or both, of the released electrons. For photoionization followed by autoionization the energy imparted to the first electron is determined by the binding energy of the primary vacancy, however. This can be used to identify the pertaining second-step spectrum.

Figure S2b shows a typical electron-electron coincidence spectrum recorded with a photon energy of 32 eV, a few eV above the inner valence ionization thresholds.

The Figure shows that a significant amount of slow electrons e_2 are recorded in coincidence with the primary 3s electrons (e_1), which have a kinetic energy of approx. 3.3 eV. Some background of electron pairs at other energies is also visible. It results from inelastic scattering of outer valence photoelectrons, and (in particular for the feature which has both electrons with kinetic energy less than 0.2 eV, upper left corner of Figure S2b) due to inelastic scattering at parts of the analyzer.

More conventional, one-dimensional electron spectra pertaining to the photoelectrons and the ICD/ETMD electrons are obtained by summing up along one of the energy axis of the two-dimensional map, and are shown in (c) and (a). The peak in Figure S2c at a
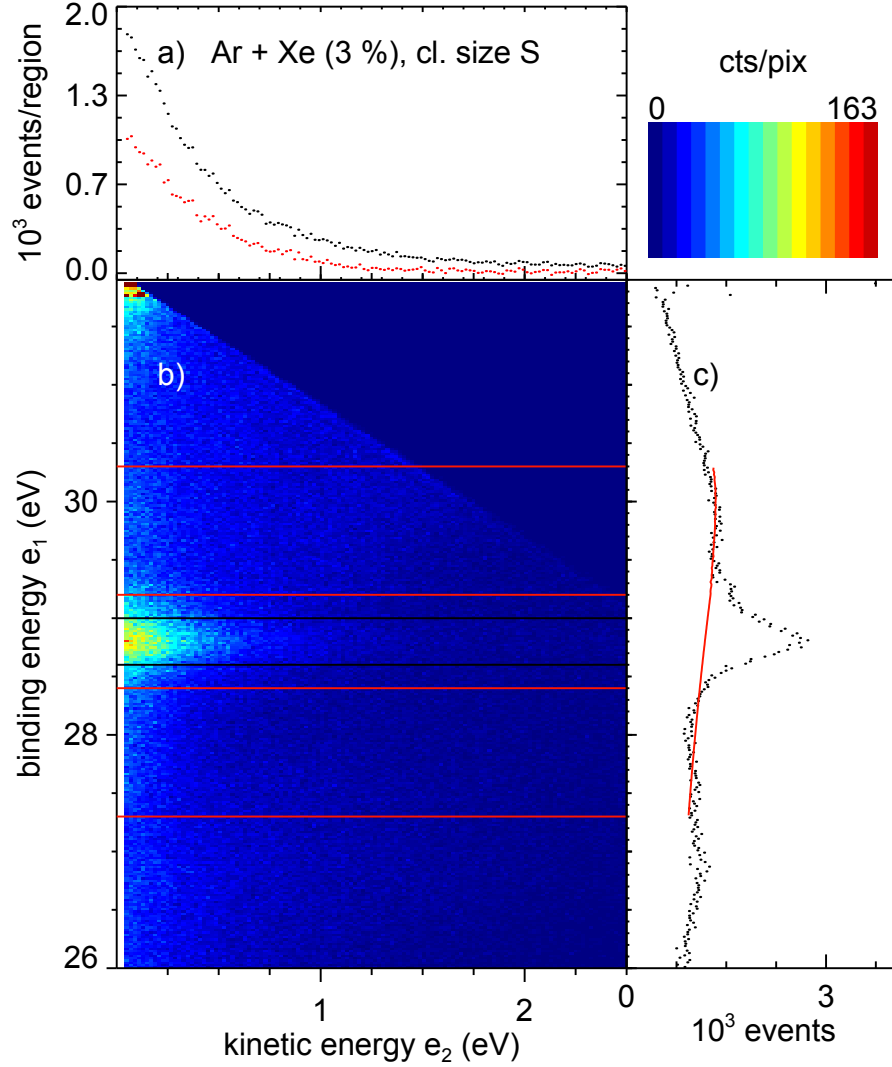
Figure S2: Photon excited electron-electron coincidence spectrum of mixed Ar-Xe clusters in the inner valence region. (b): Color-coded map of coincident electron pairs, with the electron of higher kinetic named e_1. The energy of e_1 is given as binding energy, using the photon energy of $h\nu = 32$ eV. (c): Energy spectrum of primary electrons e_1, irrespective of the energy of the secondary electron (summation of the coincidence map along horizontal lines). (a): Energy spectrum of all secondary (ICD or ETMD) electrons e_2 pertaining to the Ar 3s binding energy region marked by two black bars. See text for details. Intensity is expressed as coincident events/pixel of 20 meV^2 (b) or as coincident events per interval of 20 meV (a,c). In total, approx. 4×10^5 events are shown. The color scale of (b) is linear.

binding energy of 28.7 eV pertains to the Ar 3s photoelectron line. No atomic counterpart of this line is visible in this Figure, as only the cluster photoelectrons lead to electron-electron coincidences. The trace shown in Figure S2a is interpreted as the spectral shape of ICD/ETMD decays.

We have subtracted the background from random coincidences and coincidences due to electron scattering (electron impact ionization) from the signals shown in Figures S2a,c. In order to do so, the regions between the two pairs of red horizontal bars in Figure S2b were identified as background. The coincidence map was then subdivided into intervals of 0.5 eV width in the e_2 energy coordinate. For each interval, a second order polynomial was fitted to the background signal, and subsequently subtracted from the ICD/ETMD signal marked by the black bars. The summation of all background signals is shown as a wavy, solid red line in Figure S2c, and the signal of secondary electrons, background subtracted, is shown as the lower trace of data points in Figure S2a. Background subtracted ICD/ETMD signals are shown throughout the main paper.

These data were recorded under all expansion conditions listed in Table 1.

Similar figures were recorded for all combinations of expansion parameters listed in Table 1 of the main paper. A more detailed description of methods for analysing these data sets has been given.[?]

Experimental ICD/ETMD spectra

The background subtracted signal of secondary electrons e_2 being recorded in coincidence with a primary Ar 3s photoelectron e_1 is interpreted as the energy spectrum of ICD/ETMD of the cluster ensemble under study. Some representative examples for such spectra are shown in the main article. Here, we present a full account of these spectra. For better comparison, similar to the article they have been arranged into groups of spectra from either clusters of equal size, or of equal composition of the gas mixture (resulting in a similar ratio
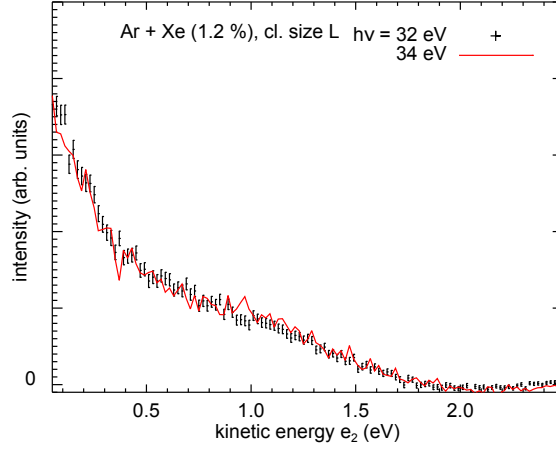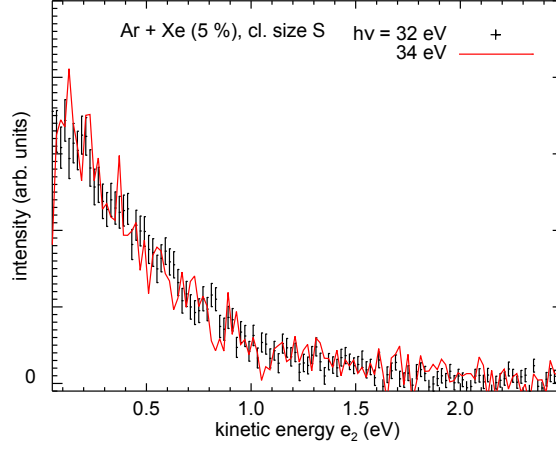
Figure S3: Energy spectrum of all coincident secondary (ICD or ETMD) electrons e_2 pertaining to primary electrons e_1 in the Ar 3s binding energy region. Spectra were recorded with photon energies of $h\nu = 32$ eV (symbols) and $h\nu = 34$ eV (trace). Spectra were normalized to equal area.

of condensed Ar to Xe, at least when averaged over the cluster ensemble). Thus, identical spectra appear more than once in the presentation.

As expected, the shape of the coincident e_2 spectra does not depend on the excitation energy (examples: Figure S3).

As discussed in the main paper, the differences between clusters of different size (Figure S4) are more substantial than those between clusters of different gas composition (Figure S5).
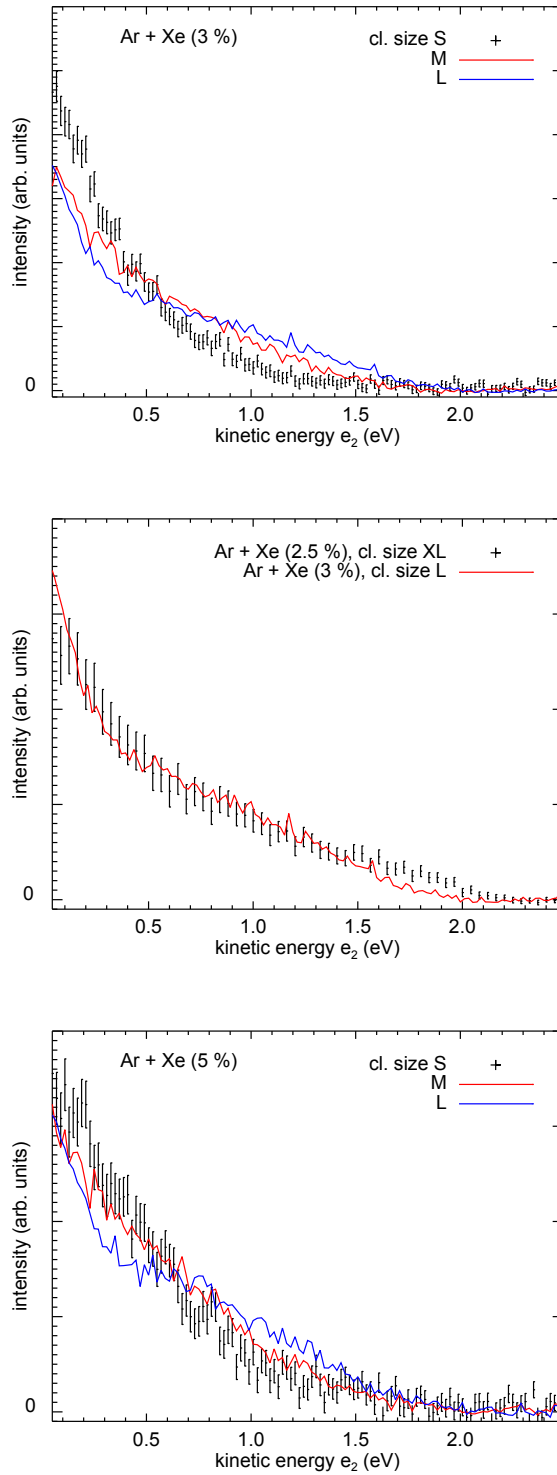
Figure S4: Energy spectrum of all coincident secondary (ICD or ETMD) electrons e_2 pertaining to primary electrons e_1 in the Ar 3s binding energy region. Comparison of the spectra from cluster ensembles of different mean size. Spectra were recorded at $h\nu = 32$ eV and were normalized to equal area.
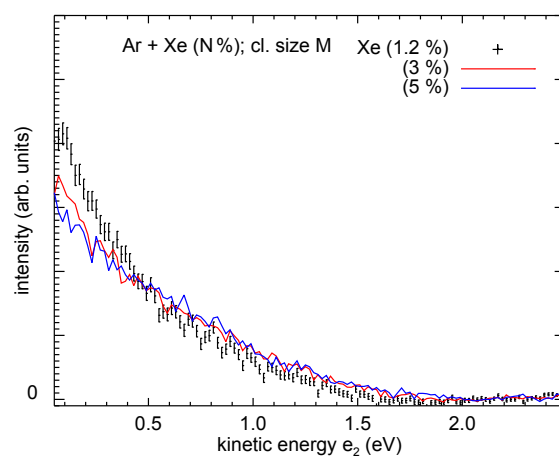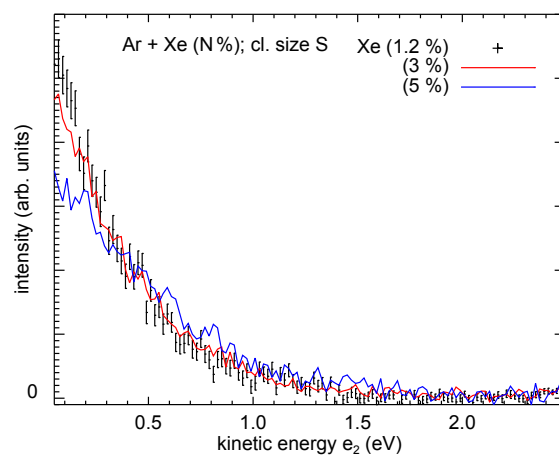
Figure S5: Comparison of the spectra from cluster ensembles of different gas composition, see Figure S4 for details.

Additional Theoretical ICD/ETMD3 Spectra

Clusters with $N = 38$ Atoms of Different Composition

Recently, structures for ArXe clusters of in total 38 atoms were optimized using an evolutionary algorithm based on two-body potentials determined by xyz.[?] In this section, the simulated ICD and ETMD3 spectra for selected cluster structures shown in Figure 7 of Ref. [?] are shown in Figures S6 – S8 and discussed.
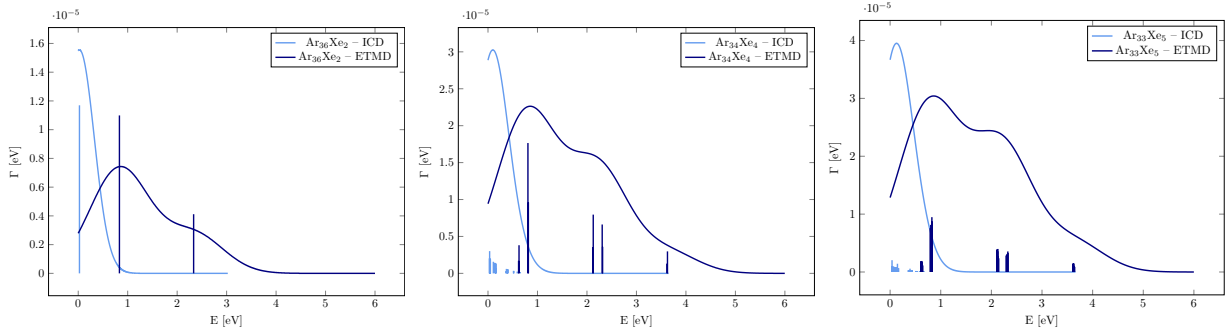

Figure S6: $Ar_N Xe_{38-N}$ clusters with a xenon content of 5% to 13%. According to our simulations the ETMD3 is the most prominent decay process for these cluster structures. In case of the $Ar_{36}Xe_2$ cluster only Xe-Xe distance is realized and therefore, the ETMD3 spectrum is very similar to one of a trimer showing two peaks originating from three different decay channels. In the other two cases the ETMD3 spectrum is slightly more complex, but in all three cases, the ETMD3 is manifested by peaks between $0.5\,eV$ and $4.0\,eV$ being in contrast to the experimental observations.
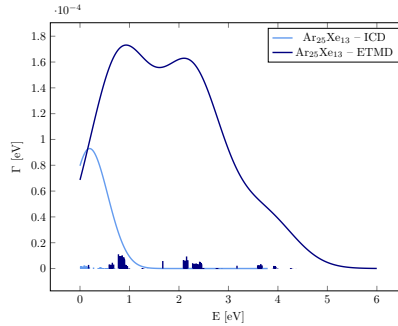

Figure S7: $Ar_2 5Xe_{13}$ clusters with a xenon content of 34%. According to our simulations the ETMD3 is the most prominent decay process for these cluster structures. In case of the $Ar_{36}Xe_2$ cluster only Xe-Xe distance is The ETMD3 is manifested by peaks between $0.5\,eV$ and $4.0\,eV$ being in contrast to the experimental observations.
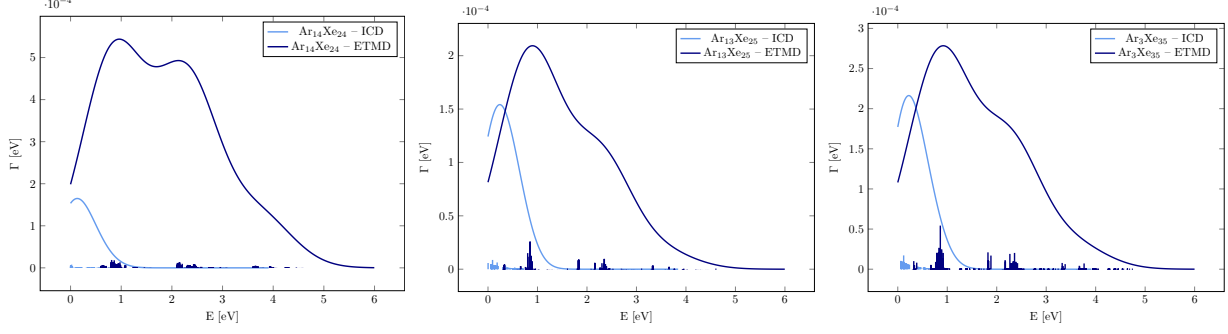
Figure S8: $Ar_N Xe_{38-N}$ clusters with a xenon content of more than 50%. Our simulations show that ETMD3 is the dominant process for these cluster structures. They are shown for completeness but can, due to the high xenon content, not be related to the experimental secondary electron measurements.

For all these cluster structures the ETMD3 is the more probable decay process and except for the $Ar_{36}Xe_2$ case with 43.6% ICD, the ETMD3 is clearly the dominant process (compare Table xyz of the main article). This can be explained by a combination of high xenon content and the scattered distribution of the xenon atoms within the cluster structures. Since the decay width of the ETMD3 is mostly caused by the decay with direct neighbours and for these $\Gamma_{ETMD3} \propto N_{Ar} N_{Xe}^2$ both the maximization of direct xenon neighbours of an argon atom and the maximization of the number of argon atoms being surrounded by xenon atoms leads to a strong increase of the ETMD3 decay width. This situation is realized in cluster structures without a seggregation of the two different elements like in the structures of Ref. At the same time, all ICD channels are closed for direct xenon neighbours. Therefore, a higher number of direct xenon neighbours for all argon atoms reduces the number of possible decay partners for a given cluster composition and therefore the ICD decay width.